Available online at www.sciencedirect.com
SCIENCE DIRECT®

Icarus 178 (2005) 19–26

ICARUS

www.elsevier.com/locate/icarus

Broadband submillimeter measurements of the full Moon center brightness temperature and application to a lunar eclipse

Juan R. Pardo[a,∗,1], Eugene Serabyn[b], Martina C. Wiedner[c,2]

[a] IEM—Departamento de Astrofísica Molecular e Infrarroja, CSIC, Serrano 121, E-28006 Madrid, Spain
[b] Division of Physics, Mathematics and Astronomy, California Institute of Technology, MS 320-47, Pasadena, CA 91125, USA
[c] Physikalisches Institut, Universität zu Köln, Zülpicherstr. 77, 50937 Köln, Germany

Received 13 December 2004; revised 16 February 2005

Available online 13 May 2005

Abstract

We report on observations of the full Moon brightness temperature covering the frequency range of 300–950 GHz, and also on observations of the lunar eclipse of July 16, 2000, though only covering the frequency range of 165–365 GHz due to poor atmospheric transmission at higher frequencies. All observations were performed from the summit of Mauna Kea (HI) using a Fourier Transform Spectrometer mounted on the Caltech Submillimeter Observatory and supplemented by measurements of the atmospheric opacity using a 183 GHz Water Vapor Monitor. The telescope was pointed to the center of the lunar disk (with a footprint of ∼45–15 km on the Moon at 300 through 900 GHz). In order to obtain the correct values of the Moon brightness temperatures at all frequencies we carefully corrected for the atmospheric absorption, which varies across the submillimeter domain. This correction is fully described. The measured pre-eclipse brightness temperature is around 337 K in the 165–365 GHz range. This temperature slightly increases with frequency to reach ∼353 K at 950 GHz, according to previous broader band data. The magnitude of the temperature drop observed during the eclipse at 265 GHz (central frequency of the band covered) was about ∼70 K, in very good agreement with previous millimeter-wave measurements of other lunar eclipses. We detected, in addition, a clear frequency trend in the temperature drop that has been compared to a thermal and microwave emission model of the lunar regolith, with the result of a good match of the relative flux drop at different frequencies between model and measurements.
© 2005 Elsevier Inc. All rights reserved.

Keywords: Moon, surface; Radio observations; Data reduction techniques

1. Introduction

The thermal radio emission of the Moon was first detected at 1.25 cm wavelength by Dicke and Beringer (1946). Subsequently, Piddington and Minnett (1949) performed a series of observations at the same wavelength over three lunar cycles. The Moon was proposed as a radiometric standard for microwave and infrared observations in the work by Linsky (1973). However, the measurements covering the accessible millimeter and submillimeter windows remain scarce, and have only been performed with different narrowband instruments at different frequencies, under different conditions and with different calibrations, making comparisons difficult. As a result, our knowledge of the exact Moon brightness temperature across the millimeter and submillimeter ranges remains poor.

In the comprehensive series of observations of the 1.25-cm emission of the Moon by Piddington and Minnett (1949) it was pointed out that the variation of the Moon's brightness temperature was roughly sinusoidal with an amplitude considerably less than the one observed for the infrared emission, measured earlier by Pettit (1935). In

∗ Corresponding author.
E-mail address: pardo@damir.iem.csic.es (J.R. Pardo).
[1] Visiting scientist at Division of Physics, Mathematics and Astronomy, California Institute of Technology, MS 320-47, Pasadena, CA 91125, USA.
[2] Visiting scientist at Harvard-Smithsonian Center for Astrophysics, 60 Garden st., ms. 78, Cambridge, MA 02138, USA.

0019-1035/$ – see front matter © 2005 Elsevier Inc. All rights reserved.
doi:10.1016/j.icarus.2005.04.005

addition, the maximum of this radio emission came about 3–1/2 days after full Moon, whereas the infrared emission shows no phase lag. The most obvious explanation for this fact is that rock-like materials (lunar regolith) in the surface consist of a layer of dust covering the rock. This was verified by Apollo-11 in 1969. The infrared emission could then be assumed to originate at the surface of the Moon, while the radio emission originates at some depth beneath the surface, where the temperature variation due to solar radiation is reduced in amplitude and shifted in phase. A multi-wavelength study across the submillimeter domain, that links the radio/millimeter with the infrared, would provide very interesting outputs to verify the thermal behavior of the lunar surface. At full Moon we would expect an increase of the temperature at shorter submillimeter wavelengths. In addition, during an eclipse we should see how the brightness temperature decreases more rapidly at shorter wavelengths (emission arising closer to the surface). This has been the motivation for monitoring the July 16, 2000, total lunar eclipse, and previous full-Moon measurements with the Fourier Transform Spectrometer (FTS) described in Serabyn and Weisstein (1996).

Measurements of the Moon brightness temperature at millimeter wavelengths during lunar eclipses have been performed in the past (Reber and Stacey, 1969; Sandor and Clancy, 1995). These have been restricted to only narrow spectral bands at wavelengths around 3.4, 1.4, and 1.3 mm. They agree on a maximum temperature drop of 25% with respect to the pre-eclipse value. However, no studies have been performed to check for a possible wavelength dependency of this temperature drop.

Here we report on submillimeter measurements of the Moon's equivalent blackbody temperature spectrum [$T_{\mathrm{EBB,Moon}}(\nu)$] across a wide range of frequencies (up to ∼800 GHz of total band) taking advantage of the dry atmosphere at Mauna Kea. Since the knowledge of the atmospheric opacity is mandatory for an accurate calibration of the FTS data, simultaneous Water Vapor Monitor (WVM) measurements were taken in three frequency bands around a water line at 183 GHz (Section 2.2), and some reference FTS atmospheric scans (as described in Serabyn et al. (1998) and Pardo et al. (2001a)), where also performed. The weather was bad during the lunar eclipse observations (Section 2) with an atmospheric water column of 5–7.5 mm allowing only FTS observations between 165 and 365 GHz. Nevertheless, a careful calibration algorithm (Section 3), based on previous developments presented in Serabyn et al. (1998), enabled us to detect the expected increase with frequency of $T_{\mathrm{EBB,Moon}}(\nu)$ across the submillimeter range at full Moon (known only between 12.5 mm and 1 mm from previous works) and the also expected (but not yet reported) frequency dependent behavior of $T_{\mathrm{EBB,Moon}}(\nu, t)$ during a lunar eclipse. These and other results are presented and discussed in Section 4. The conclusions of this work are given in Section 5.

2. Observations

For the observations two different instruments measuring full polarization were mounted on the Caltech Submillimeter Observatory (CSO): an FTS covering a wide frequency range and a WVM measuring the brightness temperature around 183 GHz. Side-by-side comparisons of these two instruments have been performed (Pardo et al., 2004).

FTS data of the full Moon were obtained on July 1, 1999, under very dry conditions (∼0.6 mm of zenith water vapor column, see Pardo et al., 2001a). This data are presented and analyzed and represent the largest frequency coverage to date of the full Moon brightness temperature at submillimeter wavelengths.

The lunar eclipse of July 16, 2000 (see Fig. 1), was monitored with the FTS between 10:35 and 14:30 UT. The weather conditions at Mauna Kea were unfortunately bad during that night with zenith precipitable water vapor ranging from 5 to 7.5 mm.

2.1. FTS observations

The basic instrumental setup of the Fourier Transform Spectrometer was described in Serabyn and Weisstein (1996). For the Moon studies different set-ups have been used. For the most favorable weather conditions, a 20″ Winston Cone (light concentrator) and a 1.1 THz low-pass filter were installed at the entrance of the bolometer, allowing us to scan the 300–1100 GHz frequency range. In July 2000, unfortunately, the weather conditions were quite adverse, and we had to select a low frequency configuration: 40″ Winston Cone and a 550 GHz low-pass filter.

The observations of the lunar eclipse were carried out as follows: We obtained several pre-eclipse Moon spectra and then we observed the eclipse taking blocks of data that consisted of 3 pairs of single-sided interferograms on the Moon and on the sky away from the Moon but at the same elevation, plus two pairs of similar scans on an ambient temperature load. For each single sided Moon scan we used a total length of 17 cm (2 and 15 cm, respectively, on the two sides of the wide light fringe position), that provided a resolution of 460 MHz. We obtained 16 such sets of observations, each of which took about 16 min. Of these data, 3.5 h of observations on the lunar eclipse are used in the discussion below, because the elevation was considered too low at the end, in particular given the large amount of water vapor present in the atmosphere (see below).

Since an accurate knowledge of the atmospheric opacity is key to perform the atmospheric correction of the Moon data (following section) we took several single-sided atmospheric scans with the FTS: 2.0 cm on one side of the white light fringe 45 cm on the other, providing the finest frequency resolution of the FTS instrument. An example of such an atmospheric measurement with the FTS and the WVM (see below) is shown on Fig. 2.

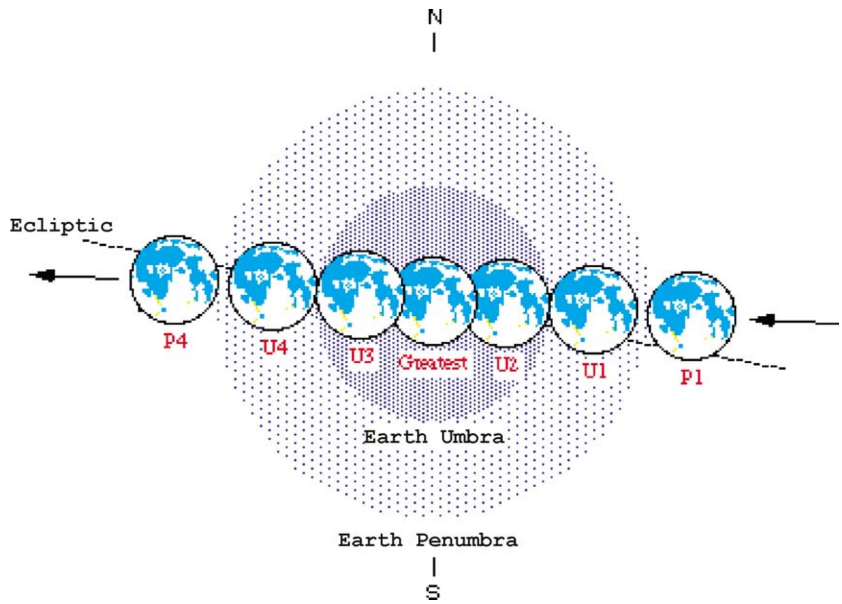

Fig. 1. 16 July 2000 total lunar eclipse. The eclipse was monitored until the Moon was at 20° elevation, slightly before U3. The eclipse diagram has been obtained from http://www.mreclipse.com/LEphoto/~TLE2000Jul16.html.

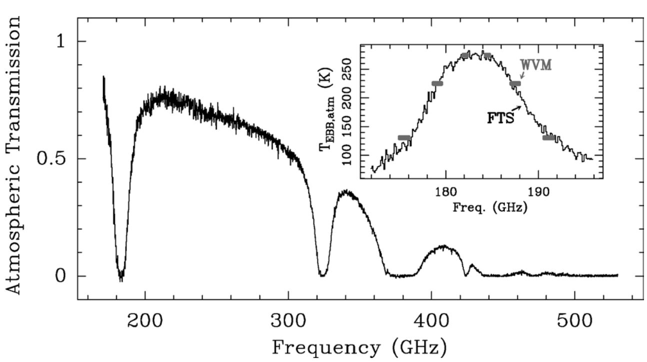

Fig. 2. FTS atmospheric transmission and water vapor monitor measurements taken on July 16, 2000, just before the lunar eclipse. Several such atmospheric measurements were carried out during the eclipse in order to perform the atmospheric correction presented in Section 3.

2.2. *WVM observations*

Besides the FTS we used a 183 GHz water vapor monitor (WVM) (see Wiedner et al., 2001) mounted on the CSO to measure the atmospheric opacity as well as to obtain an independent measurement of the Moon brightness temperature. This radiometer measures the sky brightness temperature in three double-sided channels in the wings of the 183 GHz water vapor line, 1.2, 4.2, and 7.8 GHz away from the line center. The instrument is optimized to accurately measure small changes in the sky brightness temperature with the aim of performing interferometric phase correction (Wiedner et al., 2001). It can also be used for absolute measurements of the sky brightness temperature and hence to monitor the atmospheric opacity, on time scales as short as 1 s. Both instruments provide data in good agreement (Pardo et al. (2004) and Fig. 2).

We constantly monitored the atmospheric opacity with the WVM during the observations of the lunar eclipse in order to validate the FTS atmospheric data used for the calibration of the Moon data presented in the next section. We could also clearly detect the brightness temperature changes at 183 GHz during the eclipse with the radiometer. In order not to block the FTS beam the radiometer is mounted off axis and slightly out of focus, such that the WVM points $12'$ above the telescope beam and diverges by $5'$. As the WVM sees a different region on the Moon surface than the FTS, some differences were expected, confirmed by the observations.

3. Calibration of FTS measurements of the Moon

We present in detail the calibration procedure because it presents some aspects never before described related to the large bandwidth used and the presence of the atmosphere. The atmospheric part of this calibration procedure is the same for our FTS measurements of the planets, that will be presented in future papers.

The measurement consists of interferograms (detected power vs position of the scanning mirror on the source, on the sky and on an ambient temperature load for calibration). The Fourier Transform of the interferograms gives the spectral density $S(\nu)$ in V/GHz. The measured ratio of the spectra is:

$$\mathcal{M}(\nu) = \frac{S_{\rm sou}(\nu) - S_{\rm sky}(\nu)}{S_{\rm hot}(\nu) - S_{\rm sky}(\nu)}. \tag{1}$$

Each term is:

- $$S_{\rm sou}(\nu) \equiv G(\nu)\Big\{\eta_{\rm sou}(\nu)P_{\rm sou}(\nu) + \big[\eta_{\rm sky}(\nu)-\eta_{\rm sou}(\nu)\big]P_{\rm bgr}(\nu)e^{-\tau_t(\nu)} + \big[\eta_{\rm sky}(\nu)P_{\rm sky}(\nu)+(1-\eta_{\rm sky})P_{\rm hot}(\nu)\big]\Big\},$$
- $$S_{\rm sky}(\nu) \equiv G(\nu)\Big\{\eta_{\rm sky}(\nu)\big[P_{\rm sky}(\nu)+P_{\rm bgr}(\nu)e^{-\tau_t(\nu)}\big] + \big(1-\eta_{\rm sky}(\nu)\big)P_{\rm hot}(\nu)\Big\},$$
- $$S_{\rm hot}(\nu) \equiv G(\nu)\eta_{\rm hot}(\nu)P_{\rm hot}(\nu), \qquad \eta_{\rm hot}=1.0.$$

P are the power spectra emitted by the different sources, η are the couplings to these sources (the Moon [sou], the atmosphere [sky], the ambient load [hot], and cosmic background [bgr]), τ_t is the total atmospheric opacity at the elevation of the source, and G is the optical–electrical gain factor that is eliminated with the ratio performed in Eq. (1). We thus have:

$$\mathcal{M}(\nu)=\frac{\eta_{\rm sou}(\nu)[P_{\rm sou}(\nu)-P_{\rm bgr}(\nu)]e^{-\tau_t(\nu)}}{\eta_{\rm sky}(\nu)[P_{\rm hot}(\nu)-P_{\rm sky}(\nu)-P_{\rm bgr}(\nu)e^{-\tau_t(\nu)}]}. \qquad (2)$$

Some of these sources can be considered to be blackbodies (ambient load, cosmic background). We can completely neglect the cosmic background blackbody with respect to the Moon, the atmosphere and the hot load as it always contributes less than 0.1% of the power emitted by these sources at our working frequencies:

$$\mathcal{M}(\nu)=\frac{\eta_{\rm sou}(\nu)P_{\rm sou}(\nu)e^{-\tau_t(\nu)}}{\eta_{\rm sky}(\nu)[P_{\rm hot}(\nu)-P_{\rm sky}(\nu)]}. \qquad (3)$$

The power spectrum of the atmosphere is given by the solution of the radiative transfer equation and differs significantly from a blackbody. We can nevertheless assign at each frequency that the emission of the atmosphere is that of an isothermal layer of effective temperature $T_{\rm e}(\nu)$ and emissivity $(1-e^{-\tau_t(\nu)})$. We can then rearrange Eq. (3) as follows:

$$\mathcal{M}(\nu)=\frac{\eta_{\rm sou}(\nu)P_{\rm sou}(\nu)e^{-\tau_t(\nu)}}{\eta_{\rm sky}(\nu)\mathcal{B}(T_{\rm hot})\big[1-\frac{\mathcal{B}[T_{\rm e}(\nu)](1-e^{-\tau_t(\nu)})}{\mathcal{B}(T_{\rm hot})}\big]}, \qquad (4)$$

where $\mathcal{B}$ is used to denote the mathematical formula of blackbody radiation. This is the exact calibration equation from which we can derive the power spectrum of the source (the Moon in this case). An approximation commonly used is to consider $T_{\rm e}(\nu)=T_{\rm hot}$ from which follows:

$$P_{\rm sou}(\nu)=\frac{\eta_{\rm sky}(\nu)}{\eta_{\rm sou}(\nu)}\mathcal{M}(\nu)\mathcal{B}(T_{\rm hot}). \qquad (5)$$

In order to express the spectrum of the source in a temperature scale, two different methods can be used: We can define a brightness temperature $T_{\rm B,sou}$ using a Rayleigh–Jeans approximation, or an equivalent blackbody temperature $T_{\rm EBB,sou}(\nu)$ as follows:

$$T_{\rm B,sou}(\nu)=P_{\rm sou}(\nu)\frac{c^2}{2k\nu^2}, \qquad (6)$$

$$P_{\rm sou}(\nu)=\frac{2h\nu^3/c^2}{\exp[h\nu/kT_{\rm EBB,sou}(\nu)]-1}. \qquad (7)$$

Note that:
$T_{\rm B,sou}(\nu) = T_{\rm EBB,sou}(\nu)\frac{h\nu/kT_{\rm EBB,sou}(\nu)}{\exp[h\nu/kT_{\rm EBB,sou}(\nu)]-1}$, so that they are equal in the Rayleigh–Jeans limit. We will use $T_{\rm EBB,sou}(\nu)$ in this paper.

3.1. Antenna temperature definition

We define:

$$T_{\rm A}^*(\nu)=\frac{\eta_{\rm sou}(\nu)}{\eta_{\rm sky}(\nu)}T_{\rm B,sou}(\nu). \qquad (8)$$

So that:

$$\Big[\exp\big(h\nu/kT_{\rm EBB,sou}(\nu)\big)-1\Big]^{-1}=\frac{\eta_{\rm sky}(\nu)}{\eta_{\rm sou}(\nu)}\frac{kT_{\rm A}^*(\nu)}{h\nu}. \qquad (9)$$

From the definition of $T_{\rm B,sou}(\nu)$ and Eq. (4), it follows that:

$$T_{\rm A}^*(\nu)=\mathcal{M}(\nu)T_{\rm hot}\frac{h\nu/kT_{\rm hot}}{\exp(h\nu/kT_{\rm hot})-1} \times\left[e^{\tau_t(\nu)}\left(1-\frac{\mathcal{B}[T_{\rm e}(\nu)]}{\mathcal{B}(T_{\rm hot})}(1-e^{-\tau_t(\nu)})\right)\right] \qquad (10)$$

we also define $T_{\rm a}^*(\nu)$ such as the assumption $T_{\rm e}(\nu)=T_{\rm hot}$ is valid.

$$T_{\rm a}^*(\nu)=\mathcal{M}(\nu)T_{\rm hot}\frac{h\nu/kT_{\rm hot}}{\exp(h\nu/kT_{\rm hot})-1}. \qquad (11)$$

Note that $T_{\rm A}^*(\nu)$ is obtained directly from the measured ratio $\mathcal{M}(\nu)$ and the hot load temperature, so it is very straightforward. Then, we can write:

$$T_{\rm A}^*(\nu)=T_{\rm a}^*(\nu)\cdot g(\nu),$$

where

$$g(\nu)=e^{\tau_t(\nu)}\left(1-\frac{\mathcal{B}[T_{\rm e}(\nu)]}{\mathcal{B}(T_{\rm hot})}(1-e^{-\tau_t(\nu)})\right). \qquad (12)$$

3.2. Atmospheric correction $g(\nu)$

To evaluate the correction function $g(\nu)$ we assume that the temperature of the hot load, $T_{\rm hot}$, is equal to the ambient temperature $T_{\rm sky}(0)$. We have from Serabyn et al. (1998):

$$T_{\rm e}(\tau_t)=T_{\rm hot}-LHf\big[\tau_t(\nu)\big] \qquad (13)$$

with L the tropospheric temperature lapse rate (as a positive number), H the water vapor scale height, and $f(\tau_t)\equiv\frac{\tau_t}{1-\exp(-\tau_t)}\int_0^\infty se^{-s}\exp[-\tau_t(1-e^{-s})]\,{\rm d}s$. Note that $f(0)=1$ and $\lim_{\tau_t\to\infty}f(\tau_t)=0$. $L=5.6$ K/km and $H=2$ km in average Mauna Kea conditions. Thus, $LHf(\tau_t)$ is at least $\sim$20 times smaller than $T_{\rm hot}$. This means that in the expression of $g(\nu)$ (Eq. (12)) we can apply equation B3 of Serabyn et al. (1998) to the ratio $\mathcal{B}[T_{\rm e}(\nu)]/\mathcal{B}(T_{\rm hot})$ (two blackbody func-

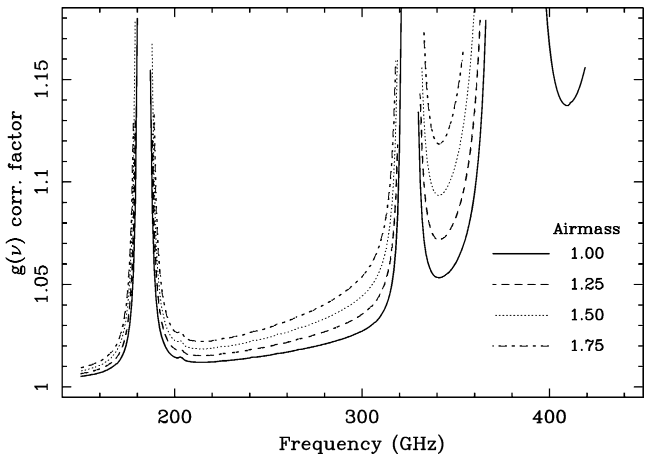

Fig. 3. $g(\nu)$ calibration correction factor below 450 GHz at different airmasses for a water vapor column of 6 mm above Mauna Kea (average conditions during the eclipse measurements). This correction has been applied to all T_a^* data in order to obtain T_A^* histograms shown in Fig. 4.

tions with similar temperatures). We then obtain:

$$g(\nu) = \left\{1 + \frac{LHf(\tau_t(\nu))h\nu/kT_{\mathrm{hot}}}{T_{\mathrm{hot}}[1 - \exp(-h\nu/kT_{\mathrm{hot}})]}(e^{\tau_t(\nu)} - 1)\right\}. \quad (14)$$

It turns out that $g(\nu) = 1 - \Delta t(\nu)e^{\tau_t(\nu)}$, where $\Delta t(\nu)$ (always a negative number) is the second order transmission correction derived in Serabyn et al. (1998) for the atmospheric transmission measurements with the same FTS ($t = t_1 + \Delta t$, where $t = e^{-\tau_t}$ is the corrected transmission and t_1 is the transmission derived under the assumption $T_e = T_{\mathrm{hot}}$). This implies $g = t_1/t$ and therefore g increases asymptotically when the true transmission t decreases.

In summary, a measurement of the atmospheric opacity spectrum (with the FTS) allows to calculate the correction factor g to be applied to $T_a^*(\nu)$ (straightforward curve obtained from the measured ratio $\mathcal{M}(\nu)$) to obtain the corrected curve $T_A^*(\nu)$ from which the equivalent blackbody spectrum of the source, $T_{\mathrm{EBB,sou}}(\nu)$, can be obtained, provided that the ratio $\frac{\eta_{\mathrm{sky}}(\nu)}{\eta_{\mathrm{sou}}(\nu)}$ is known (assumed to be 1.0 here due to the large angular size of the source $\eta_{\mathrm{sou}} = 1.0$ and the use of the same aperture mask described in Serabyn et al. (1998) so that $\eta_{\mathrm{sky}} = 1.0$).

From the above discussion it follows that the calibration errors in T_a^* dramatically increase when the water vapor increases, when the elevation decreases and/or when the frequency is close to atmospheric lines. Our radiative transfer code ATM (Pardo et al., 2001b) has been used to show how big these corrections are in the case of the lunar eclipse data at different elevations (Fig. 3).

4. Results

4.1. Background

The Moon is mainly seen in reflected light from the Sun at optical wavelengths. On the other hand, at very long wavelengths (radio) the radiation has its origin at some depth below the surface. In the millimeter and submillimeter range, the thermal emission still largely dominates but the depth from which it arises changes with frequency (becoming closer to the surface as it increases). For our experiment, this should result on two effects:

1. At full Moon the brightness temperature should increase with frequency due to less penetration.
2. During a lunar eclipse the equivalent blackbody temperature should drop faster at higher frequencies due to the heat conductivity of the lunar soil (temperature drop slower as the depth increases) and the penetration (deeper for longer wavelengths).

Lawson et al. (2000), using the Clementine long-wave infrared camera operating at 8.75 µm found that the brightness temperature of the sub-solar point at that wavelength averaged 380 K, whereas Monstein (2001) found at 2.77 cm wavelength a value of 210 K averaged over the Moon disk for the full Moon. These values should be taken as upper and lower limits for our experiment.

4.2. Submillimeter full Moon spectrum: frequency behavior

The Moon scans taken on July 1, 1999, have been reduced by applying the $g(\nu)$ curve obtained from the atmospheric spectrum presented in Pardo et al. (2001a) as reference. T_a^* clearly shows the atmospheric opacity effect expected. After its correction, all scans, independently of the airmass, are consistent in T_A^* within the noise, that goes from ∼10–15 K at around 250–350 GHz to ∼1–3 K above 550 GHz (Fig. 4). The T_A^* spectrum is basically flat with an average value of 330 K. This translates into Equivalent Blackbody temperatures ranging from 337 K at ∼250 GHz to 353 K at ∼950 GHz. The latest value is quite close from the one found by Eve et al. (1977) for the sub-solar point in the 350 µm atmospheric window (around 360 K).

M. De Petris (private communication) has calculated the central full Moon brightness temperature for our measured spectral range following the review model published in Mangum (1993) based on Krotikov and Troitskii (1964) and Linsky (1966, 1973). The main assumption is that the lunar surface is smooth and uniform with depth-independent thermal properties. Details on the model parameters can be found in Section 5 of Mangum (1993). The agreement of this model with our measurements is quite good (see Fig. 4) with may be just a small overestimate of the model with respect to the data around 650 GHz.

4.3. The Moon brightness temperature during a lunar eclipse

During the observations of the lunar eclipse the frequency coverage was only ∼165–365 GHz as a result of the sky conditions (Section 2) and the noise was around 5 K, below 2%

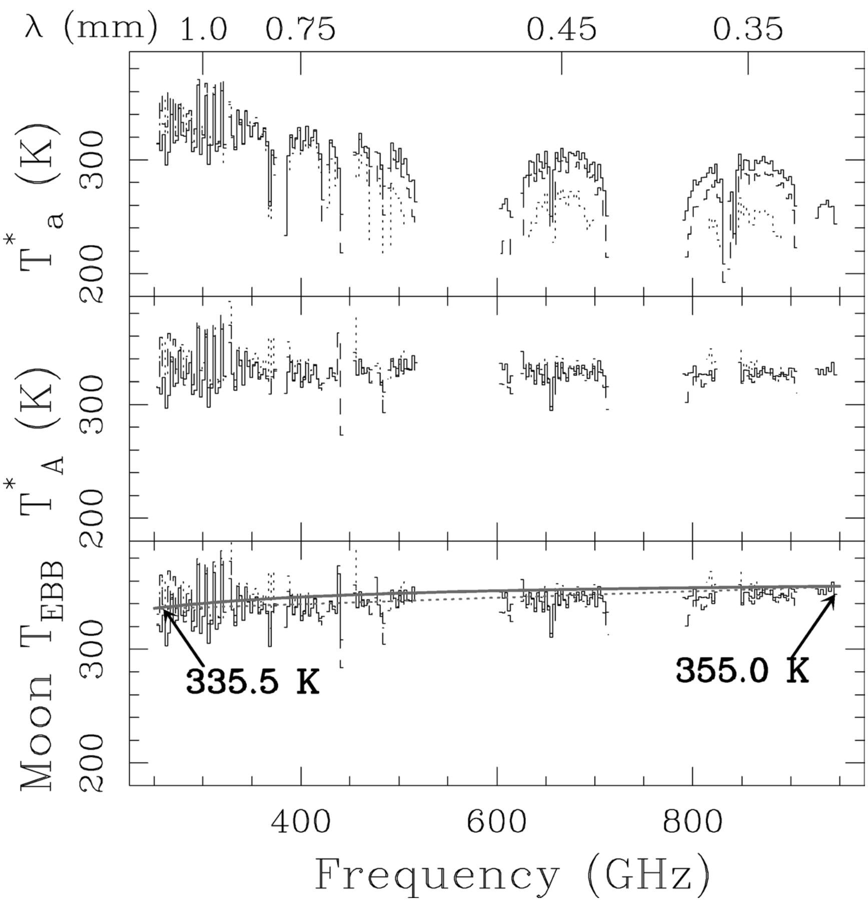

Fig. 4. Calibration sequence applied to three FTS measurements of the Moon obtained at different elevations on July 1, 1999, with the FTS installed at the CSO. The three step ($\mathcal{M} \to T_a^* \to T_A^* \to T_{EBB}^*$) calibration procedure described in this paper perfectly removes the discrepancies related to zenith atmospheric opacity and airmass (1.0, 1.4, and 1.8 here). The higher noise around 1 mm is due to the low transmission around that wavelength of the beam splitter used for these measurements. The solid gray line represents model calculations made by M. De Petris (see text) and the dotted line is just a straight line connecting the extremes of the model curve.

of the measured flux at all frequencies (see Fig. 5). The pre-eclipse data compare very well with the July 1, 1999, data: the brightness temperature at 250 GHz is basically the same. No slope can be seen due to the small frequency coverage (200 GHz). As the eclipse progressed, the expected behavior, i.e. greater temperature drop at higher frequencies during the eclipse due to the thermal emission arising from closer to the surface, is confirmed (Fig. 5).

The measured ratio of the total flux respect to the pre-eclipse value has been compared for two frequencies (240 and 350 GHz) with results from Stephen J. Keihm model calculations (see Keihm (1984) and references therein) for this particular eclipse at the lunar disk center. The model considers a dielectric loss tangent (ratio between the imaginary and real parts of the dielectric constant of the soil) of 0.008. The agreement is quite good, and the effect of the faster drop in brightness temperature at 350 GHz respect to 240 GHz is evident. Only the last data point clearly departs from the model. A low signal-to-noise ratio due to the low elevation is the most possible explanation. We decided not to use the data obtained afterward.

Sandor and Clancy (1995) followed a lunar eclipse at 225 GHz at the center of the lunar disk and other locations. It is not clear that the amount they give as "brightness temperature" is equivalent to our T_{EBB} defined above. In any case they observe a maximum decrease of their measured flux with respect to the pre-eclipse value of 25%, compared to ∼18% at 240 GHz and ∼32% at 350 GHz in our case just until the beginning of totality. The decrease should continue after that moment but slowing down according to the above model.

5. Summary

In this work we have performed the first broadband fully calibrated measurements of the submillimeter brightness temperature of the Moon (total frequency range: 165–950 GHz). Several steps and the help of atmospheric transmission measurements are necessary to convert the measured fluxes on the Moon, the sky and an ambient load into the equivalent blackbody temperature of the center of the Moon. The calibration scheme has been presented in detail.

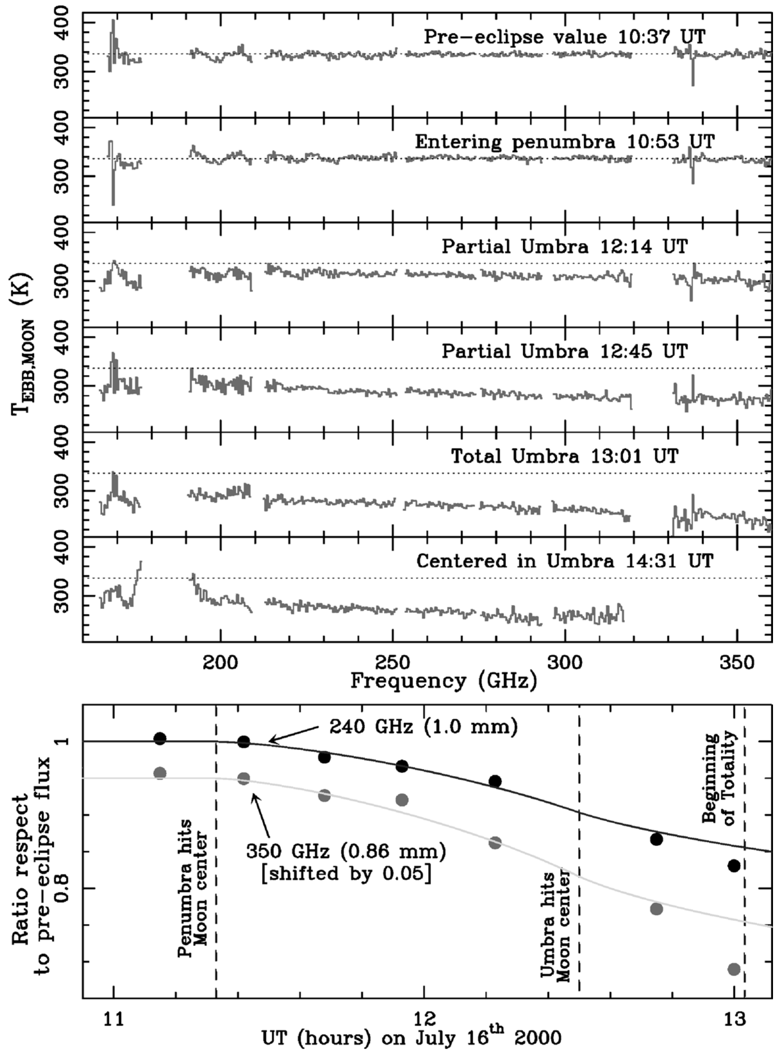

Fig. 5. Upper panel: equivalent blackbody temperatures at the center of lunar disk measured during the July 16, 2000, total lunar eclipse. Lower panel: time evolution of the flux ratio with respect to the pre-eclipse values at 240 and 350 GHz compared with model results (see text). The noise in the measured flux ratios is 0.02 or smaller.

The full Moon data are of interest to reduce observations of the giant planets performed with the same FTS. This analysis is presently in progress.

The full Moon data show a slight $T_{\rm EBB}$ increase with frequency and in general agrees well with model calculations and lots of scattered measurements in narrow frequency bands routinely performed by millimeter and submillimeter telescopes for calibration purposes. The values found here benefit from the fact that a total bandwidth of $\sim$800 GHz has been covered simultaneously, reduced with the same criteria, and that the atmospheric transmission has been taken into account carefully. Therefore, the values found are proposed as reference for calibration purposes.

Finally, the instrument and data reduction technique were applied to follow a lunar eclipse. Unfortunately the weather conditions were far from ideal and the useful frequency range was reduced to only 165–365 GHz. Nevertheless, expected behaviors of the Moon $T_{\rm EBB}$ as a function of frequency and as the eclipse progressed could be verified in general terms. Available configurations of the FTS instrument could at present allow to follow an eclipse in the 300–1100 GHz range, weather permitting. The results presented here certainly encourage such an experiment to learn more about the thermal behavior of the lunar soil beyond 300 GHz, where observations are scarce.

Acknowledgments

We are grateful to Drs. M. De Petris and S.J. Keihm for providing their model calculations for comparison to our data. The authors wish to thank the CSO Hawaii staff for providing assistance during the observations. This work has been supported by NSF Grants ATM-9616766 and AST-9615025, and by Spanish MCyT Grants ESP2002-01627, AYA2002-10113-E and AYA2003-02785-E. CSO operations were supported by NSF Grant AST-9980846.

References

Dicke, R.H., Beringer, R., 1946. Microwave radiation from the Sun and Moon. Astrophys. J. 103, 375–376.

Eve, W.D., Sollner, T.C.L.G., Robson, E.I., 1977. Submillimetre lunar emission. Astron. Astrophys. 59, 209–213.

Keihm, S.J., 1984. Interpretation of the lunar microwave brightness temperature spectrum—feasibility of orbital heat flow mapping. Icarus 60, 568–589.

Lawson, S.L., Jakosky, M., Park, H.-S., Mellon, M.T., 2000. Brightness temperatures of the lunar surface: Calibration and global analysis of the Clementine long-wave infrared camera data. J. Geophys. Res. 105-E2, 4273–4290.

Krotikov, V.D., Troitskii, V.S., 1964. Radio emission and nature of the Moon (Engl. Transl.). Sov. Phys. Uspeskhi 6, 841–871.

Linsky, J.L., 1966. Models of the lunar surface including temperature-dependent thermal properties. Icarus 5, 606–634.

Linsky, J.L., 1973. The Moon as a proposed radiometric standard for microwave and infrared observations of extended sources. Astrophys. J. 216 (Suppl. Ser.), 163–203.

Mangum, J.G., 1993. Main-beam efficiency measurements of the Caltech Submillimeter Observatory. Publ. Astron. Soc. Pacific 105, 117–122.

Monstein, C., 2001. The Moon's Temperature at $\lambda = 2.77$ cm. http://e-collection.ethbib.ethz.ch/ecol-pool/bericht/bericht_87.pdf.

Pardo, J.R., Serabyn, E., Cernicharo, J., 2001a. Submillimeter atmospheric transmission measurements on Mauna Kea during extremely dry El Niño conditions: Implications for broadband opacity contributions. J. Quant. Spectros. Radiat. Trans. 68, 419–433.

Pardo, J.R., Cernicharo, J., Serabyn, E., 2001b. Atmospheric transmission at microwaves (ATM): An improved model for millimeter/submillimeter applications. IEEE Trans. Antenn. and Propag. 49 (12), 1683–1694.

Pardo, J.R., Wiedner, M.C., Cernicharo, J., Wilson, C.D., Cunningham, C., Hills, R.E., Serabyn, E., 2004. Side-by-side comparison of Fourier transform spectroscopy and water vapor radiometry as tools for the calibration of millimeter/submillimeter ground-based observatories. Astrophys. J. S 153, 363–367.

Pettit, E., 1935. Lunar radiation as related to phase. Astrophys. J. 81, 17–37.

Piddington, J.H., Minnett, H.C., 1949. Microwave thermal radiation from the Moon. Aust. J. Sci. Res. 2, 63–77.

Reber, E.E., Stacey, J.M., 1969. 1.4-mm and 3.4-mm observations of the lunar eclipse on 18 October 1967. Icarus 10, 171–178.

Sandor, B.J., Clancy, R.T., 1995. Microwave observations and modeling of a lunar eclipse. Icarus 115, 387–398.

Serabyn, E., Weisstein, E.W., 1996. Calibration of planetary brightness temperature spectra at near-millimeter and submillimeter wavelengths with a Fourier transform spectrometer. Appl. Opt. 35, 2752–2763.

Serabyn, E., Weisstein, E.W., Lis, D.C., Pardo, J.R., 1998. Submillimeter Fourier transform spectrometer measurements of atmospheric opacity above Mauna Kea. Appl. Opt. 37, 2185–2198.

Wiedner, M.C., Hills, R.E., Carlstrom, J.E., Lay, O.P., 2001. Interferometric phase correction using 183 GHz water vapor monitors. Astrophys. J. 553, 1036–1041.